SUPPLEMENTARY FIGURE 1

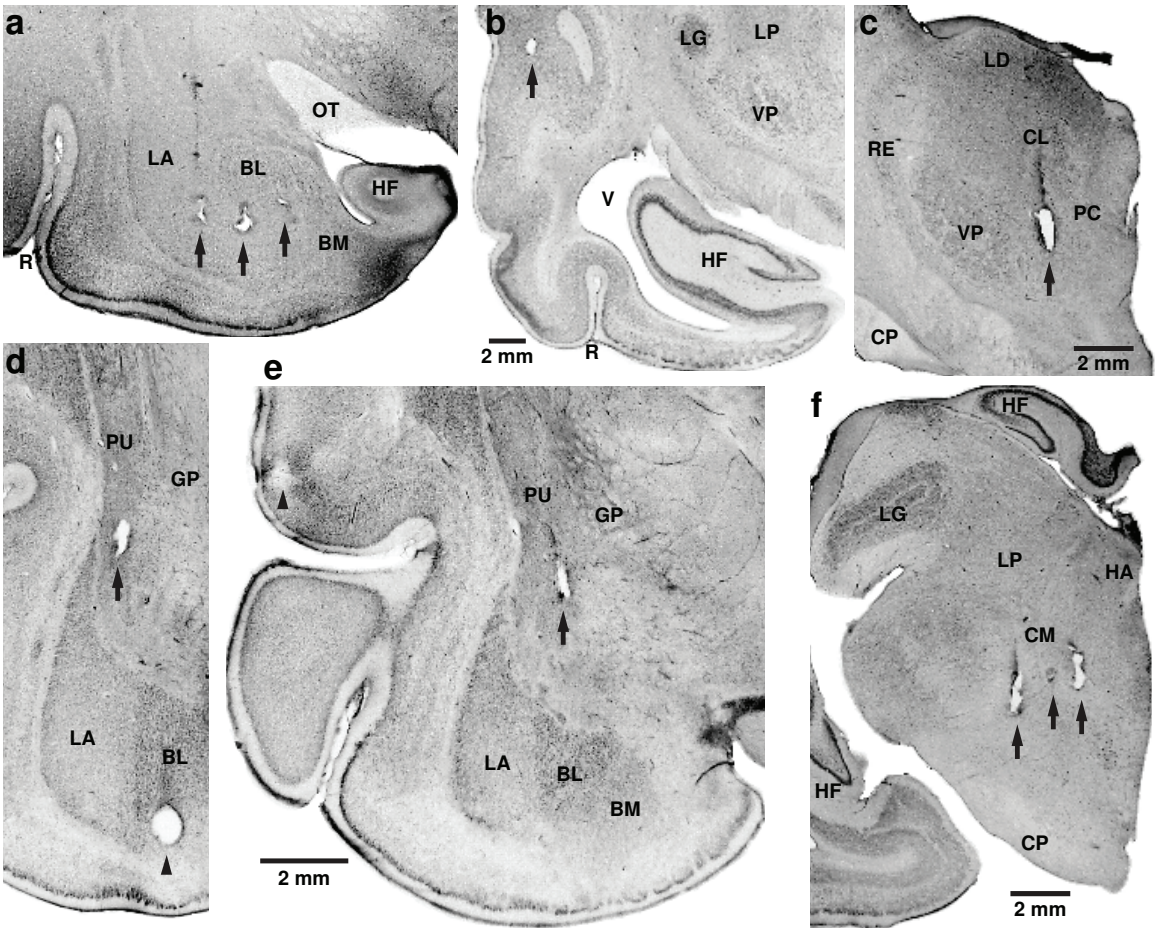

Supplementary Fig. 1 Histological verification of recording sites. Coronal sections stained with cresyl violet. Arrows and arrowheads point to electrolytic lesions performed at the end of the experiments to mark the last recording sites in the BLA (**a, d)**, primary and secondary auditory cortices (**b, e**), rostral and caudal intralaminar nuclei (**c, f),** as well as putamen **(d, e)**. Scale bar in **e** also valid for panels **a** and **d**. Abbreviations: BL, basolateral amygdaloid nucleus; BM, basomedial amygdaloid nucleus; CL, central lateral thalamic nucleus; CM, central medial thalamic nucleus; CP, cerebral peduncle; GP, globus pallidus; HA, habenula; HF, hippocampal formation; LA, lateral nucleus of the amygdala; LG, lateral geniculate nucleus of the thalamus; LP, lateroposterior thalamic nucleus; OT, optic tract; PC, paracentral thalamic nucleus; PU, putamen; R, rhinal sulcus; RE, reticular thalamic nucleus; V, ventricle; VP, ventroposterior thalamic nucleus.

SUPPLEMENTARY FIGURE 2

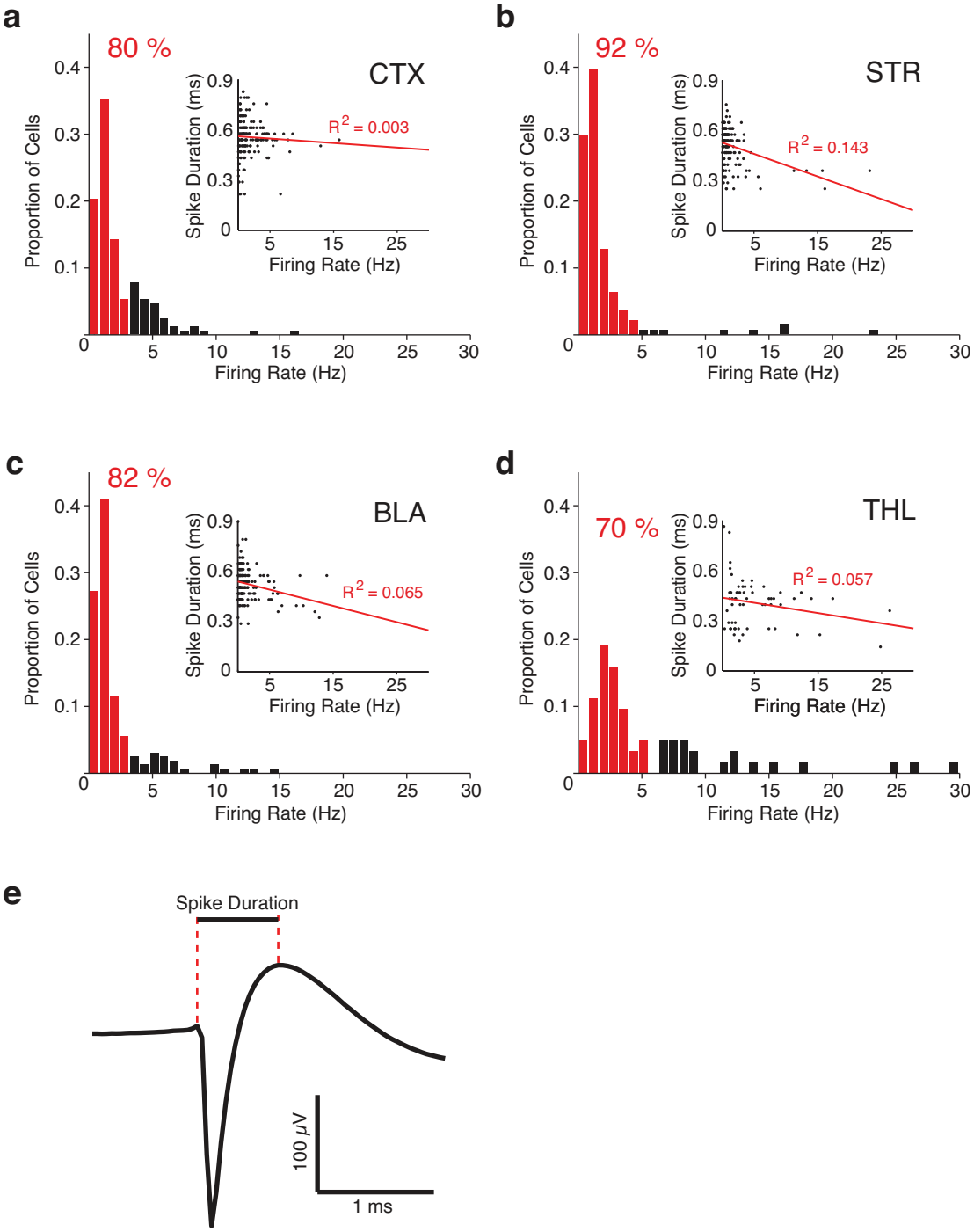

Supplementary Fig. 2 Firing rates and spike durations in the cortical, striatal, BLA, and thalamic neurons included in the present study. Following spike sorting, we measured the baseline firing rate and average spike duration of each recorded unit. (**a-d**) Frequency distribution of firing rates in cortical (**a**, n = 159), striatal (**b** , n = 139), BLA (**c**, n = 152), and thalamic (**d**, n = 55) neurons. **Insets** in **a-d** plot spike duration (y-axis) as a function of firing rate (x-axis). As shown in **e**, spike duration was defined as the interval between the onset of the negative component of the spike to the peak of the subsequent positivity. Frequency distributions of firing rates revealed evidence of heterogeneity in our samples. Therefore, we ignored neurons whose firing rates fell outside the peak of the distributions.

SUPPLEMENTARY FIGURE 3

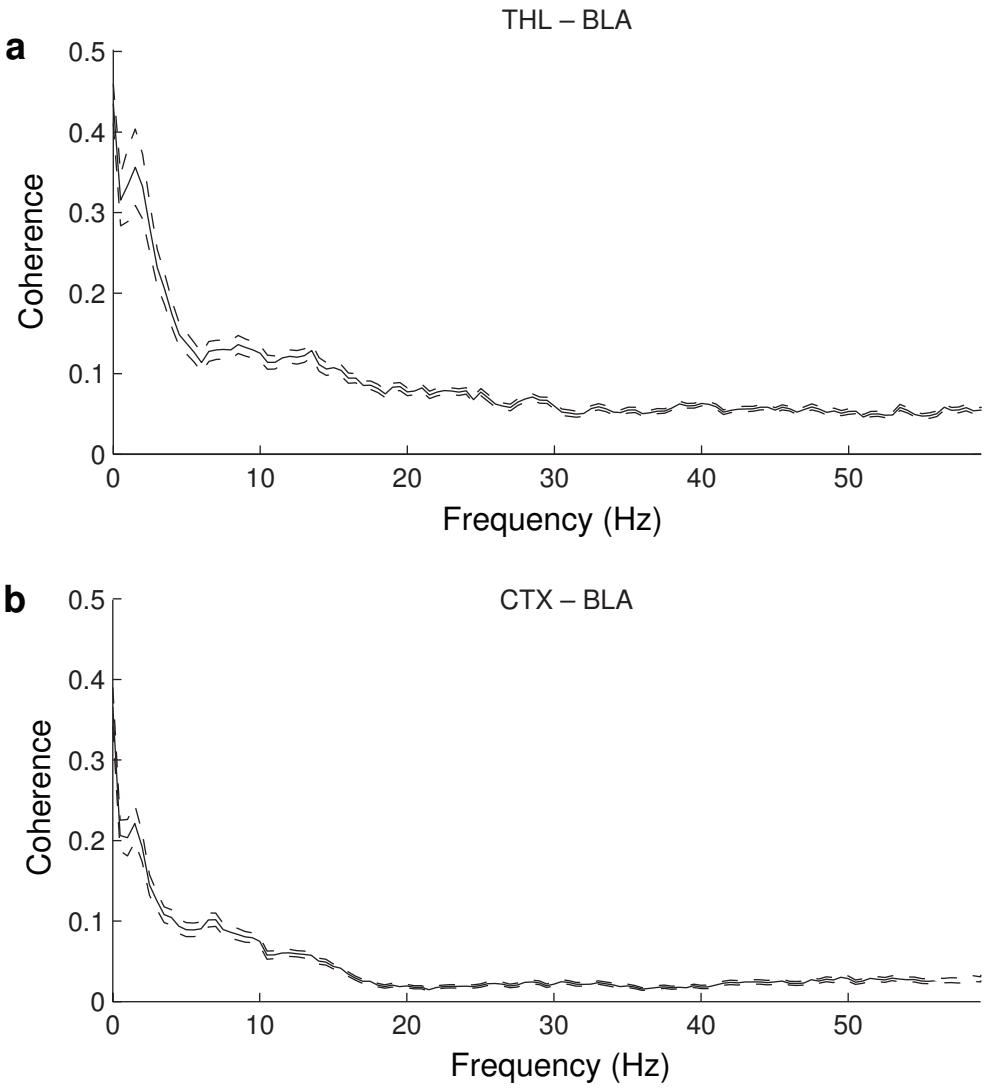

Supplementary Fig. 3 Frequency dependence of the coherence between LFPs simultaneously recorded in the BLA and thalamus (a) or BLA and cortex (b). Plots of coherence (y-axis; average ± SEM) vs. frequency (Hz). Dashed lines indicate SEM.

SUPPLEMENTARY FIGURE 4

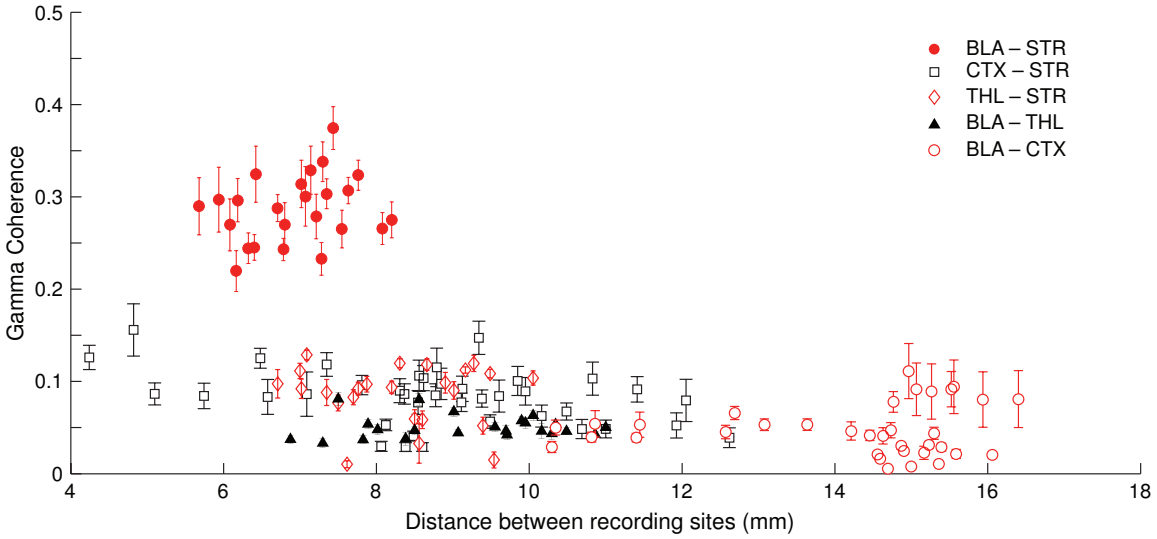

Supplementary Fig. 4 Impact of distance between recording sites on gamma coherence. Gamma coherence (y-axis; average ± SEM) plotted as a function of distance between recording sites (x-axis) for various combinations of recorded structures, as indicated in the legend shown in the upper right. BLA-striatal gamma coherence (solid red circles) is higher than seen with all other combinations of recorded structures, even when only considering pairs of recording sites separated by the same distance.

SUPPLEMENTARY FIGURE 5

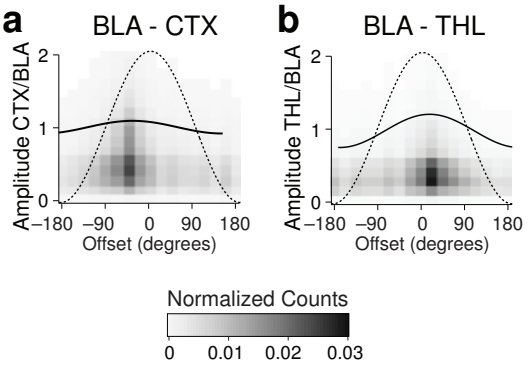

Supplementary Fig. 5 Normalized frequency distributions of phase lags (x-axis) between BLA vs. cortical (**a**) or thalamic (**b**) gamma as a function of normalized gamma amplitude (left y-axis). The lines overlaid on these graphs represent the average gamma cycles seen at the corresponding sites (BLA, dashed lines; cortical and thalamic, solid lines).

SUPPLEMENTARY FIGURE 6

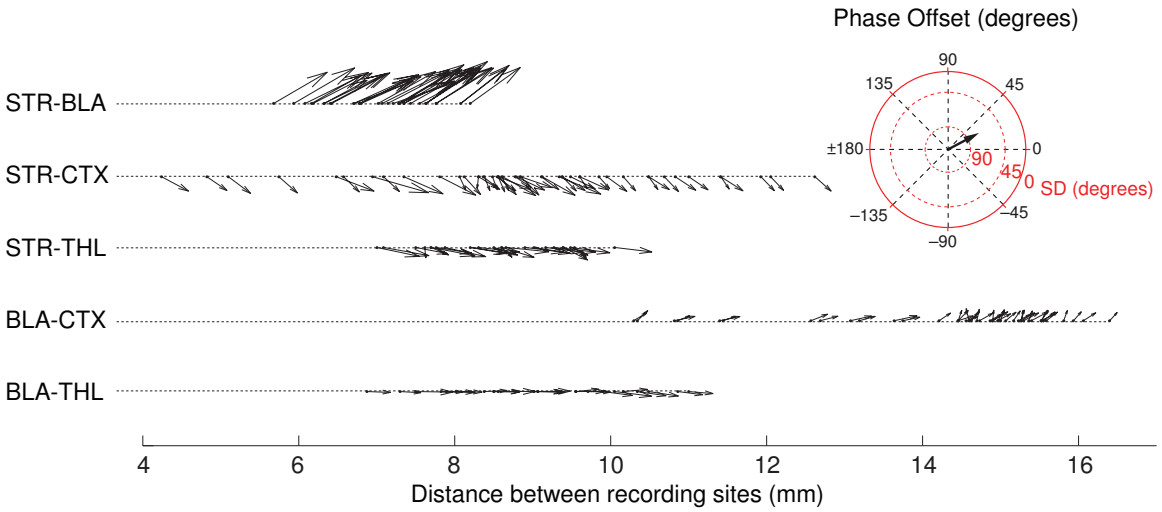

Supplementary Fig. 6 Impact of distance between recording sites on phase offset between gamma oscillations. **Angle** of arrows indicates average phase relation (see polar plot for legend). **Origin** of arrows indicates distance between recording sites (refer to x-axis). **Length** of arrows is inversely proportional to standard deviation of phase offset (the shorter the arrows, the higher the variability). Here, a perfectly fixed cycle-to-cycle phase relationship would have been ascribed a value of 1. The length of the arrows was computed using conventional vector averaging techniques (refer to red in polar plot for correspondence).

SUPPLEMENTARY FIGURE 7

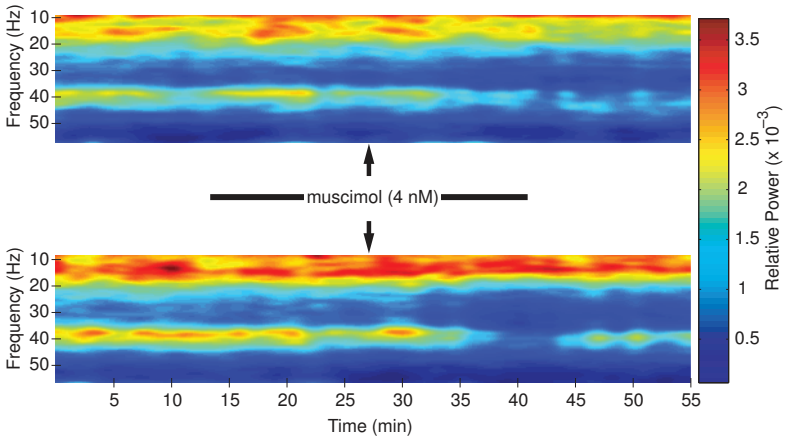

Supplementary Fig. 7 Intra-BLA muscimol infusions reduce striatal gamma power in individual cats. Striatal LFP power (color-coded) in different frequencies (y-axis) plotted as a function of time (x-axis) in experiments where muscimol was slowly infused in the BLA over a period of 25 min. Two examples of this test, performed in different cats, are shown.

SUPPLEMENTARY FIGURE 8

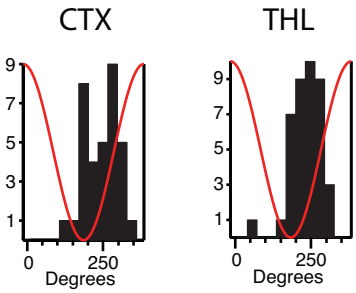

Supplementary Fig. 8 Frequency distributions of firing peak times for thalamic (**left**) and cortical (**right**) neurons in relation to gamma activity picked up by the same electrode as that used for the unit recordings.

SUPPLEMENTARY FIGURE 9

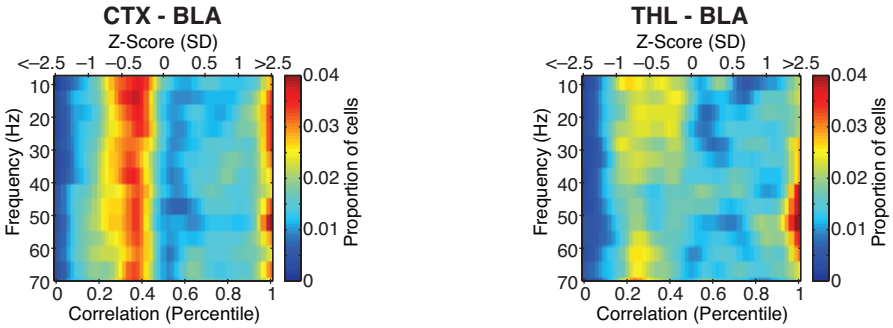

Supplementary Fig. 9 Same analysis as in figure 3i-k but for cortical and BLA (**left**) or thalamic and BLA (**right**) neurons. Color-coded frequency distributions of correlation indices of central 10 ms of crosscorrelograms (x-axis) plotted as a function the frequency of BLA LFPs (y-axis) used to select spikes included in the crosscorrelograms. The bottom x-axis expresses the data in percentiles. The correspondence in Z-scores can be found in the top x-axis.

SUPPLEMENTARY FIGURE 10

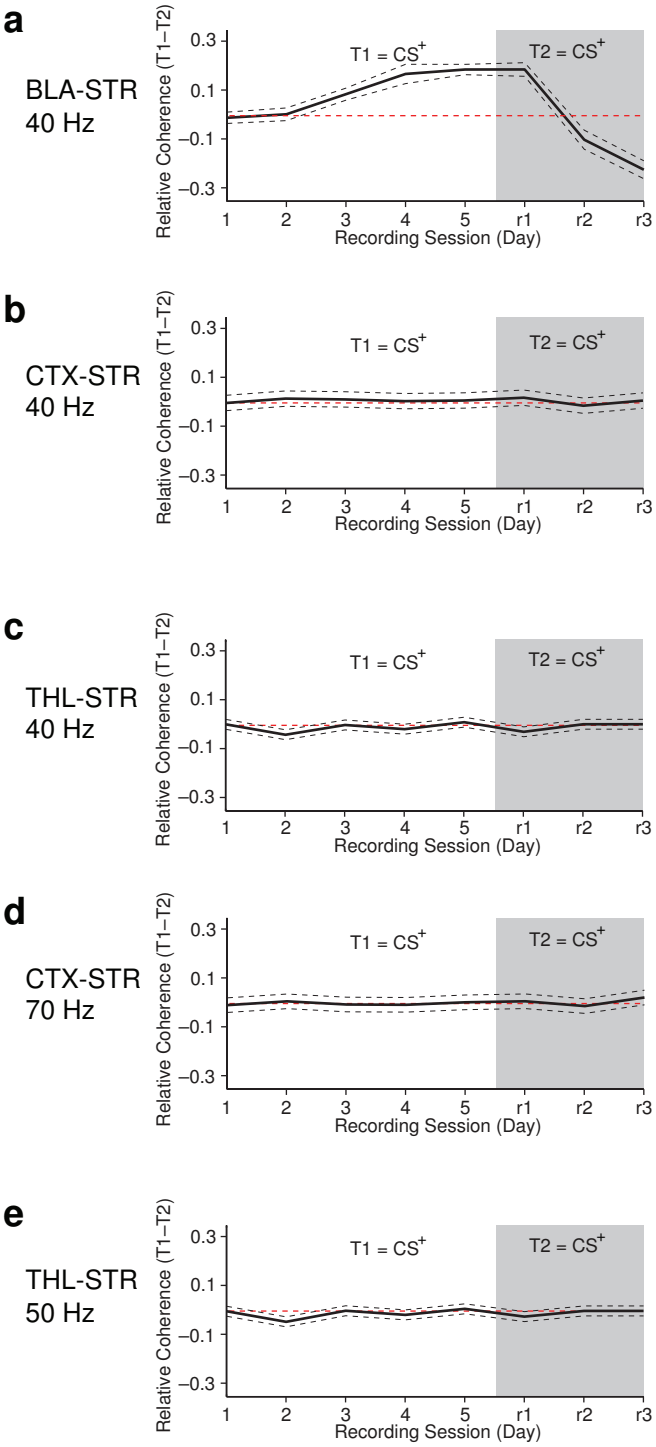

Supplementary Fig. 10 Learning-related changes in correlated gamma are seen only between BLA and striatum, not between striatal and cortical or striatal and thalamic recording sites. For all panels, the y axis plots the difference in coherence elicited by the two tones (y-axis) as a function of recording sessions (x-axis). Panels a-c examines fluctuations in gamma coherence between striatal and BLA (**a**), striatal and cortical (**b**), or striatal and thalamic (**c**) recording sites. **(d-e)** Learning-related fluctuations in coherence of 70 Hz (**d**) or 50 Hz (**e**) LFP activity in cortical and striatal (**d**) or thalamic and striatal (**e**) recording sites, respectively. In all cases dashed gray lines indicate SEM.